EXTENDED KALMAN FILTER FOR ESTIMATION OF CONTACT FORCES AT WHEEL-RAIL INTERFACE

Khakoo Mal
PhD Scholar, Department of Electronic Engineering,
Mehran University of Engineering and Technology, Jamshoro, (Pakistan).
E-mail: 17phdiict05@students.muet.edu.pk ORCID: https://orcid.org/0000-0002-5754-0441

Imtiaz Hussain
Associate Professor, Electrical Engineering.
DHA Suffa University. Karachi, (Pakistan).
E-mail: imtiaz.hussain@dsu.edu.pk ORCID: https://orcid.org/0000-0002-7947-9178

Bhawani Shankar Chowdhry
Professor Emeritus.
Mehran University of Engineering and Technology. Jamshroo, (Pakistan).
E-mail: bhawani.chowdhry@faculty.muet.edu.pk ORCID: https://orcid.org/0000-0002-4340-9602

Tayab Din Memon
Associate Professor, Department of Electronics.
Mehran University of Engineering and Technology. Jamshoro, (Pakistan).
E-mail: tayabdin82@gmail.com ORCID: https://orcid.org/0000-0001-8122-5647

Recepción: 20/01/2020 **Aceptación:** 15/04/2020 **Publicación:** 30/04/2020

Citación sugerida Suggested citation

Mal , K., Hussain, I., Chowdhry, B. S., y Memon, T. D. (2020). Extended Kalman filter for estimation of contact forces at wheel-rail interface. *3C Tecnología. Glosas de innovación aplicadas a la pyme. Edición Especial, Abril 2020,* 279-301. http://doi.org/10.17993/3ctecno.2020.specialissue5.279-301

ABSTRACT

The wheel-track interface is the most significant part in the railway dynamics because the forces produced at wheel-track interface governs the dynamic behavior of entire vehicle. This contact force is complex and highly non-linear function of creep and affected with other railway vehicle parameters. The real knowledge of creep force is necessary for reliable and safe railway vehicle operation. This paper proposed model-based estimation technique to estimate non-linear wheelset dynamics. In this paper, non-linear railway wheelset is modeled and estimated using Extended Kalman Filter (EKF). Both wheelset model and EKF are developed and simulated in Simulink/MATLAB.

KEYWORDS

Railway dynamics, Wheel-rail interface, Model-based estimation, Extended Kalman Filter.

http://doi.org/10.17993/3ctecno.2020.specialissue5.279-301

1. INTRODUCTION

The main element of any study of rolling stock behavior is the wheel-track interaction patch (Simon, 2006). All the forces which help and direct the railway vehicle transmit via this narrow area of contact and knowing of the nature of these forces is most important for any investigation of the generic railway vehicle behavior (Melnik & Koziak, 2017).

The Wheel-track condition information can be detected in real time to provide traction and braking control schemes for re-adhesion. For example, in Charles, Goodall and Dixon (2008) an indirect technique based on Kalman Filter (KF) is proposed for the estimation of low adhesion with wheel-track profile by using conicity and wheel-rail contact forces. A method using Kalman filter has also been introduced in Mei, Yu and Wilson (2008) and Hussain and Mei (2009) to identify the slip after evaluating the torsional frequencies in the axle of wheelset. Two indirect monitoring schemes using a bank of Kalman filters are proposed for (i) wheel slip detection and, (ii) real time contact condition and adhesion estimation in Hussain and Mei (2010, 2011). In Hussain, Mei and Ritchings (2013) and Ward, Goodall and Dixon (2011), the development of techniques based on Kalman-Bucy filter proposed for the estimation of wheel-track interface conditions in real time to predict the track and wheel wear, the development of rolling contact fatigue and any regions of adhesion variations or low adhesion.

However, due to nonlinear nature of wheel-rail dynamic behavior, Kalman-Bucy filter is difficult to use for entire operating conditions. A method using Heuristic non-linear contact model and Kalker's linear theory is proposed in Anyakwo, Pislaru and Ball (2012) for modeling and simulation of dynamic behavior of wheel-track interaction in order to discover the shape of interaction patch and for obtaining the tangential interaction forces generated in wheel-rail interaction area. On the basis of measurement of traction motor's parameters, (i) creep forces can be predicted by means of Kalman filter between roller and wheel (Zhao, Liang & Iwnicki, 2012) and (ii) slip-slide is detected and estimated by using Extended Kalman Filter (EKF) (Zhao & Liang, 2013).

A system based on two different processing methods, i.e., model-based approach using Kalman-Bucy filter and non-model based using direct data analysis, is presented for on-board indirect detection of low adhesion condition in Hubbard *et al.* (2013a, 2013b).

http://doi.org/10.17993/3ctecno.2020.specialissue5.279-301

However, the technique using yaw acceleration as a normalization method provides only a rough estimate and introduces a huge delay to obtain an estimate. A model-based technique using Unscented Kalman Filter (UKF) is proposed by Zhao *et al.* (2014) for estimation of creep, creep forces as well as friction coefficient from the behavior of traction motor. However estimators seem unreliable in some critical track conditions, hence still work is needed to monitor these wheel-rail parameters more effectively in real time.

A system based on the principles of synergetic control theory is proposed in Radionov and Mushenko (2015) to estimate adhesion moment in wheel-track contact point. Two-dimensional inverse wagon model based on acceleration is developed in Sun, Cole and Spiryagin (2015) for evaluation and monitoring of wheel-rail contact dynamics forces. The results at higher speed are agreeable, however improvement in the model is further needed to reduce the error at all expected speeds. Another technique using multi-rate EKF state identification is presented in Wang *et al.* (2016) for detection of slip velocity by merging the multi-rate technique and Extended Kalman filter technique to identify the load torque of traction motor. On the basis of fitting non-linear model, EKF can also be applied to identify the wheel-track interaction forces and moments that takes into account the interface nonlinearities (Strano & Terzo, 2018).

After reviewing the literature on condition monitoring of railway wheelset dynamics, it is observed that the problem to analyze wheelset conditions and update them to desired situation still needs to be improved in order to accomplish the expectation of railway vehicle to be really high speed, high comfort, more safer and economical means of transport across the world.

In this paper, Extended Kalman filter is designed for non-linear railway wheelset model to estimate lateral velocity and yaw rate of wheelset as well as creep and creep force. Polach formulae for creep force and friction coefficient are used in modeling of non-linear wheelset. Both modeling of non-linear wheelset and designing of EKF are done in Simulink/MATLAB.

http://doi.org/10.17993/3ctecno.2020.specialissue5.279-301

2. MODELING OF NON-LINEAR WHEELSET

The motion of a railway vehicle is directed by interaction forces produced at wheel-track contact, which change non linearly with respect to creepage and are affected by the unpredictable variations in the adhesion conditions (Hussain, 2012). A single solid-axle wheelset shown in Figure 1 is taken for modeling and estimation of wheel-rail conditions.

Figure 1. Railway wheelset [captured by author during field visit].

The creepages (the relative speed of the wheel to rail) of right and left wheels of wheels in longitudinal direction are expressed in following equations.

$$\gamma_{xR} = \frac{\left(r_0\omega_R - v\right)}{v} - \frac{L_g\Psi'}{v} - \frac{\omega_R\lambda_w\left(y - y_t\right)}{v} \tag{1}$$

$$\gamma_{xL} = \frac{\left(r_0\omega_L - v\right)}{v} - \frac{L_g\Psi'}{v} - \frac{\omega_L\lambda_w\left(y - y_t\right)}{v} \tag{2}$$

The main objective of this paper is to develop a state of art technique to detect the changes in wheel-rail contact conditions. The term $\frac{\left(r_0\omega_R - v\right)}{v}$ in equations (1) and (2) does not involve lateral and yaw dynamics, hence can be excluded in simplified longitudinal creep equations because only yaw and lateral dynamics are sufficient for detecting these changes. Further , so the simplified creep equations used in above model become as:

$$\gamma_{xR} = -\frac{L_g\Psi'}{v} - \frac{\lambda_w\left(y - y_t\right)}{r_0} \tag{3}$$

$$\gamma_{xL} = -\gamma_{xR} = \frac{L_g\Psi'}{v} + \frac{\lambda_w\left(y - y_t\right)}{r_0} \tag{4}$$

http://doi.org/10.17993/3ctecno.2020.specialissue5.279-301

The creepages in lateral direction are expressed as:

$$\gamma_{yR} = \gamma_{yL} = \gamma_y = \frac{y'}{v} - \Psi \tag{5}$$

While in equations (6) total creep of the wheels is depicted.

$$\gamma_{i=\sqrt{\gamma_{ji}^{\ 2} + \gamma_{ji}^{\ 2}}} \tag{6}$$

As the wheel-rail contact forces govern railway vehicle's dynamics are creep forces and are the function of creeps. The adhesion coefficient is the ratio of tangential force that is creep force to normal force and hence is also a function of creep. Figure 2 illustrates a classic nonlinear change of the adhesion coefficient with respect to creepage for all track conditions i.e. dry, wet, poor and worst conditions.

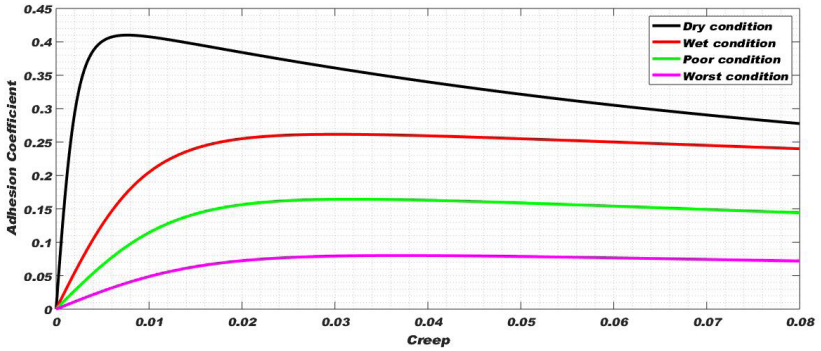

Figure 2. Creep v/s Adhesion Coefficient for all conditions of wheel-rail interface.

Following equations illustrate creep forces and adhesion coefficient.

$$F_{ji} = \frac{F_i \gamma_{ji}}{\gamma_i} \tag{7}$$

i = Right and left wheels, j = longitudinal and lateral directions

F_i is the total creep force and can be calculated by Polach formula (Polach, 2005).

http://doi.org/10.17993/3ctecno.2020.specialissue5.279-301

$$F = \frac{2\mathrm{NU}}{}\left[\frac{\mathrm{k}_A}{1+(\mathrm{k}_A)^2} + \arctan\left(\mathrm{k}_S\right)\right] \tag{8}$$

Where U is friction coefficient, is gradient of the tangential stress in area of adhesion, k_A is reduction factor in the area of adhesion and is the reduction factor in slip. Both U and are illustrated as:

$$U = u_0\left[\left(1-A\right)e^{(-B\gamma\mathrm{v})} + A\right] \tag{9}$$

Where u_0 is maximum friction coefficient at zero creep velocity, A is ratio of friction coefficient at infinity creep velocity to u_0 and B is coefficient of exponential friction decrease.

$$= \frac{2}{3}\frac{a^2 b\mathrm{c}}{\mathrm{NU}}\gamma \tag{10}$$

While a and b are half-axes of contact ellipse and c is coefficient of contact shear stiffness in $\mathrm{N/m^3}$.

$$\mu = \frac{F}{N} \tag{11}$$

The equations of motion of railway wheelset at any point of creep curve of Figure 2 are expressed as (Hussain and Mei, 2009):

$$M_v\mathrm{x}'' = F_{xR} + F_{xL} \tag{12}$$

$$m_w y'' = -F_{yR} - F_{yL} + F_C \tag{13}$$

$$I_w\Psi'' = F_{xR}L_g - F_{xL}L_g - K_w\Psi \tag{14}$$

$$\mathrm{T}_s = \mathrm{K}_s\theta_s + C_S\left(\omega_R - \omega_L\right) \tag{15}$$

$$\mathrm{I}_L\omega'_L = \mathrm{T}_s - \mathrm{T}_L \tag{16}$$

$$\mathrm{I}_R\omega'_R = \mathrm{T}_m - \mathrm{T}_s - \mathrm{T}_R \tag{17}$$

Where $\theta_s = \int\left(\omega_R - \omega_L\right)\mathrm{dt}$

http://doi.org/10.17993/3ctecno.2020.specialissue5.279-301

F_C is centripetal force component and can be neglected when vehicle does not run in curves and C_S is material damping of shaft which is normally very small. Hence both terms are not considered in this research.

In Table 1 detailed information of all parameters used in simulated wheelset model is given.

Table 1. Parameters used in modeling on non-linear wheelset.

No.	Symbol	Parameter	Value	Unit
1	γ_{xR}	Right wheel creep in longitudinal direction	calculated	ratio
2	γ_{xL}	Left wheel creep in longitudinal direction	calculated	ratio
3	γ_{yR}	Right wheel creep in lateral direction	calculated	ratio
4	γ_{yL}	Left wheel creep in lateral direction	calculated	ratio
5	γ_R	Total creep of right wheel	calculated	ratio
6	γ_L	Total creep of left wheel	calculated	ratio
7	r_0	Wheel radius	0.5 (constant)	m
8	L_g	Half gauge of track	0.75 (constant)	m
9	λ_w	Wheel conicity	0.15 (constant)	rad
10	ω_L	Angular velocity of left wheel	calculated	rad/sec
11	ω_R	Angular velocity of right wheel	calculated	rad/sec
12	v	Vehicle's forward velocity	calculated	m/sec
13	y	Lateral displacement	Output	m
14	y_t	Track disturbance in lateral direction	input	m
15	Ψ	Yaw angle	output	rad
16	F_{xR}	Right wheel creep force in longitudinal direction	calculated	Newton
17	F_{xL}	Left wheel creep force in longitudinal direction	calculated	Newton
18	F_{yR}	Right wheel creep force in lateral direction	calculated	Newton
19	F_{yL}	Left wheel creep force in lateral direction	calculated	Newton
20	F_R	Total creep force of right wheel	calculated	Newton
21	F_L	Total creep force of left wheel	calculated	Newton
22	μ	Adhesion coefficient between track and wheel	calculated	ratio
23	N	Normal load on wheel	constant	Newton
24	M_v	Vehicle mass	15000 (constant)	Kg
25	I_w	Yaw moment of inertia of wheelset	700 (constant)	Kgm^2
26	K_w	Yaw stiffness	$5x10^6$ (constant)	N//rad
27	m_w	Wheel weight with induction motor	1250 (constant)	Kg
28	v_0	Vehicle's forward velocity at initial	input	m/sec
29	ω_0	Angular velocity of wheelset at initial	input	Rad/sec
30	T_m	Torque of traction motor	input	Nm
31	T_s	Torsional torque	calculated	Nm
32	T_R	Traction torque on right wheel	calculated	Nm

http://doi.org/10.17993/3ctecno.2020.specialissue5.279-301

No.	Symbol	Parameter	Value	Unit
33	T_L	Traction torque on left wheel	calculated	Nm
34	I_R	Right wheel inertia	134 (constant)	Kgm^2
35	I_L	Left wheel inertia	64 (constant)	Kgm^2
36	K_s	Torsional stiffness	6063260 (constant)	N/m
37	θ_s	Twist angle	calculated	rad

3. DESIGNING OF EXTENDED KALMAN FILTER FOR ESTIMATING NON-LINEAR WHEELSET MODEL

Being non-linear nature of railway wheelset model, it is difficult to estimate the wheelset dynamics with ordinary estimation techniques. Therefore Extended Kalman filter is used to estimate wheelset dynamics and contact force in all adhesion conditions. Kalman filter utilizes measurements associated to the state and error covariance matrices to produce a gain known as Kalman gain. Figure 3 shows the block diagram of Kalman filter with generic scheme.

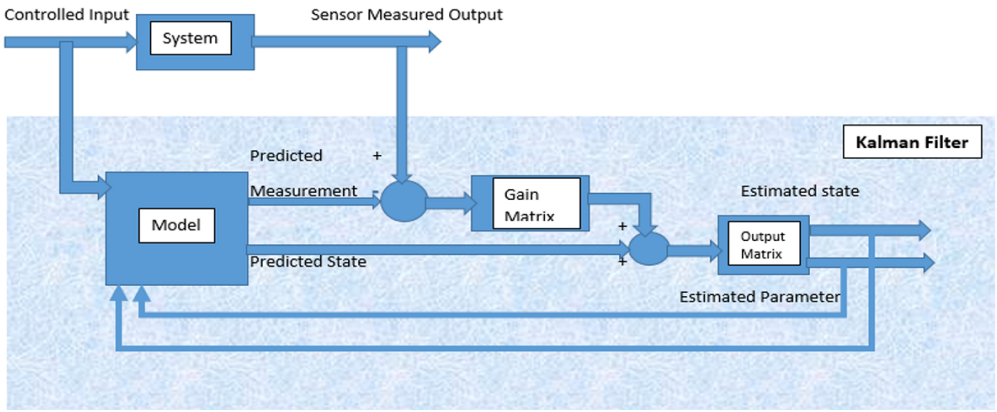

Figure 3. Block diagram of the Kalman filter with generic scheme.

Extended Kalman filter (the extension form of Kalman filter) linearizes the current mean and covariance by assessing Jacobian matrices and their partial derivatives (Ngigi *et al.*, 2012)

From non-linear model of railway wheelset, single equation (18) in matrix form is furnished after putting the values of F_{xR}, F_{xL}, F_{yR} and F_{yL} in equations (13) and (14).

http://doi.org/10.17993/3ctecno.2020.specialissue5.279-301

$$\begin{bmatrix} y' \\ \Psi' \\ y'' \\ \Psi'' \end{bmatrix} = \begin{bmatrix} 0 & 0 & 1 & 0 \\ 0 & 0 & 0 & 1 \\ 0 & \frac{1}{m_w}\left(\frac{F_R}{\gamma_R}+\frac{F_L}{\gamma_L}\right) & -\frac{1}{m_w v}\left(\frac{F_R}{\gamma_R}+\frac{F_L}{\gamma_L}\right) & 0 \\ -\frac{L_g\lambda_w}{I_w r_0}\left(\frac{F_R}{\gamma_R}+\frac{F_L}{\gamma_L}\right) & -\frac{k_w}{I_w} & 0 & -\frac{L_g^{\,2}}{I_w v}\left(\frac{F_R}{\gamma_R}+\frac{F_L}{\gamma_L}\right) \end{bmatrix} \begin{bmatrix} y \\ \Psi \\ y' \\ \Psi' \end{bmatrix} + \begin{bmatrix} 0 \\ 0 \\ 0 \\ \frac{L_g}{I_w r_0}\left(\frac{F_R}{\gamma_R}+\frac{F_L}{\gamma_L}\right) \end{bmatrix} y_t \quad (18)$$

If left and right wheel creep are same ($\gamma_R = \gamma_L = \gamma$ and $F_R = F_L = F$) then

$$\begin{bmatrix} y' \\ \Psi' \\ y'' \\ \Psi'' \end{bmatrix} = \begin{bmatrix} 0 & 0 & 1 & 0 \\ 0 & 0 & 0 & 1 \\ 0 & \frac{2}{m_w}\frac{F}{\gamma} & -\frac{2}{m_w v}\frac{F}{\gamma} & 0 \\ -\frac{2L_g\lambda_w}{I_w r_0}\frac{F}{\gamma} & -\frac{k_w}{I_w} & 0 & -\frac{2L_g^{\,2}}{I_w v}\frac{F}{\gamma} \end{bmatrix} \begin{bmatrix} y \\ \Psi \\ y' \\ \Psi' \end{bmatrix} + \begin{bmatrix} 0 \\ 0 \\ 0 \\ \frac{2L_g}{I_w r_0}\frac{F}{\gamma} \end{bmatrix} y_t \quad (19)$$

Here are state variables of wheelset model i.e y'(lateral velocity), Ψ' (Yaw rate) γ (Creep or slip), U (friction coefficient) and F (Creep force) taken for EKF algorithm. Lateral acceleration (y'') and yaw rate (Ψ'') can be measured along noise with accelerometer and gyroscope. From equation (19):

$$y'' = (y')' = \frac{2}{m_w}\left(\Psi\frac{F}{\gamma} - \frac{y'}{v}\frac{F}{\gamma}\right) \quad (20)$$

$$\Psi'' = (\Psi')' = \frac{1}{I_w}\left(\frac{2y_t L_g}{r_0}\frac{F}{\gamma} - \frac{2yL_g\lambda_w}{r_0}\frac{F}{\gamma} - \frac{2\Psi' L_g^{\,2}}{v}\frac{F}{\gamma} - K_w\Psi\right) \quad (21)$$

$$\gamma = \sqrt{\left(\frac{L_g\Psi'}{v} + \frac{\lambda_w(y - y_t)}{r_0}\right)^2 + \left(\frac{y'}{v} - \Psi\right)^2} \quad (22)$$

$$U_k = u_0[(1-A)e^{(-B\gamma v)} + A] \quad (23)$$

$$F = \frac{2NU}{1+(k_A)^2}\left[\frac{k_A}{1+(k_A)^2} + \arctan(k_S)\right] \quad (24)$$

http://doi.org/10.17993/3ctecno.2020.specialissue5.279-301

Now it is required to discretize equations (20)-(24) by using Forward Euler (FE) method in order to design Extended Kalman filter for estimation.

$$y'_k = y'_{k-1} + \frac{2\tau}{m_w}\left(\Psi\frac{F_{k-1}}{\gamma_{k-1}} - \frac{y'_{k-1}}{\mathrm{v}}\frac{F_{k-1}}{\gamma_{k-1}}\right) \tag{25}$$

$$\Psi'_k = \Psi'_{k-1} + \frac{\tau}{I_w}\left(\frac{2\mathrm{y}_t\mathrm{L}_g}{r_0}\frac{F_{k-1}}{\gamma_{k-1}} - \frac{2\mathrm{yL}_g\lambda_w}{r_0}\frac{F_{k-1}}{\gamma_{k-1}} - \frac{2\Psi'_{k-1}\mathrm{L}_g{}^2}{r_0}\frac{F_{k-1}}{\gamma_{k-1}} - K_w\Psi\right) \tag{26}$$

$$\gamma_k = \sqrt{\left(\frac{L_g\Psi'_{k-1}}{v} + \frac{\lambda_w(\mathrm{y}-y_t)}{r_0}\right)^2 + \left(\frac{y'_{k-1}}{v} - \Psi\right)^2} \tag{27}$$

$$U_k = u_0[(1-A)e^{(-B\gamma_{k-1}\mathrm{v})} + A] \tag{28}$$

$$F_k = \frac{2\mathrm{NU}_{k-1}}{}\left[\frac{\mathrm{k}_A\frac{2}{3}\frac{a^2bc}{\mathrm{NU}_{k-1}}\gamma_{k-1}}{1+(\mathrm{k}_A\frac{2}{3}\frac{a^2bc}{\mathrm{NU}_{k-1}}\gamma_{k-1})^2} + \arctan\left(\mathrm{k}_S\frac{2}{3}\frac{a^2bc}{\mathrm{NU}_{k-1}}\gamma_{k-1}\right)\right] \tag{29}$$

As the Extended Kalman filter uses a 2 step predictor-corrector algorithm (Welch & Bishop, 2001). The predictor step is given by

$$\hat{x}_k^- = f\left(\hat{x}_{k-1}, u_k, k\right) \tag{30}$$

$$P_k^- = F_{k-1}P_{k-1}F_{k-1}^T + Q_k \tag{31}$$

And the equations of corrector step are,

$$K_k = P_k^- H_k^T\left(H_k P_k^- H_k^T + R_k\right)^{-1} \tag{32}$$

$$\hat{x}_k = \hat{x}_k^- + K_k\left(\tilde{y}_k - h\left(x\hat{}_k^-, u_k, k\right)\right) \tag{33}$$

$$P_k = \left(I - K_k H_k\right)P_k^- \tag{34}$$

Where f and h are non-linear functions relating to process and measurement states, while:

http://doi.org/10.17993/3ctecno.2020.specialissue5.279-301

$$F_k = \frac{\partial f}{\partial x}|\hat{x}_k, u_k, k \text{ and } H_k = \frac{\partial h}{\partial x}|\hat{x}_k, u_k, k$$

Nomenclature of EKF algorithm is given in below table.

Table 2. Nomenclature of EKF algorithm.

Symbol	Description
x^-k	discretized a-priori estimated process
x^k	discretized a-postriori estimated process
Pk-	a-priori estimate of the covariance of process error
Pk	estimate of the covariance of measurement error
Fk	Jacobian matrix of process
Hk	Jacobian matrix of measurement
Qk	process noise covariance
Rk	measurement noise covariance
Kk	Kalman gain
ỹk	measured output

The Jacobean matrix of process matrix:

$$x_k = \begin{bmatrix} y'_k \\ \Psi'_k \\ \gamma_k \\ U_k \\ F_k \end{bmatrix} \text{ is}$$

$$F_k = \begin{bmatrix} \frac{\partial y'_k}{\partial y'_k} & \frac{\partial y'_k}{\partial \psi'_k} & \frac{\partial y'_k}{\partial \gamma_k} & \frac{\partial y'_k}{\partial U_k} & \frac{\partial y'_k}{\partial F_k} \\ \frac{\partial \psi'_k}{\partial y'_k} & \frac{\partial \psi'_k}{\partial \psi'_k} & \frac{\partial \psi'_k}{\partial \gamma_k} & \frac{\partial \psi'_k}{\partial U_k} & \frac{\partial \psi'_k}{\partial F_k} \\ \frac{\partial \gamma_k}{\partial y'_k} & \frac{\partial \gamma_k}{\partial \psi'_k} & \frac{\partial \gamma_k}{\partial \gamma_k} & \frac{\partial \gamma_k}{\partial U_k} & \frac{\partial \gamma_k}{\partial F_k} \\ \frac{\partial U_k}{\partial y'_k} & \frac{\partial U_k}{\partial \psi'_k} & \frac{\partial U_k}{\partial \gamma_k} & \frac{\partial U_k}{\partial U_k} & \frac{\partial U_k}{\partial F_k} \\ \frac{\partial F_k}{\partial y'_k} & \frac{\partial F_k}{\partial \psi'_k} & \frac{\partial F_k}{\partial \gamma_k} & \frac{\partial F_k}{\partial U_k} & \frac{\partial F_k}{\partial F_k} \end{bmatrix} \quad (35)$$

http://doi.org/10.17993/3ctecno.2020.specialissue5.279-301

And the Jacobian matrix of measurement matrix $m_k = \begin{bmatrix} y''_k \\ \Psi'_k \end{bmatrix}$ is

$$H_k = \begin{bmatrix} \frac{\partial y''_k}{\partial y'_k} & \frac{\partial y''_k}{\partial \Psi'_k} & \frac{\partial y''_k}{\partial \gamma_k} & \frac{\partial y''_k}{\partial U_k} & \frac{\partial y''_k}{\partial F_k} \\ \frac{\partial \Psi'_k}{\partial y'_k} & \frac{\partial \Psi'_k}{\partial \Psi'_k} & \frac{\partial \Psi'_k}{\partial \gamma_k} & \frac{\partial \Psi'_k}{\partial U_k} & \frac{\partial \Psi'_k}{\partial F_k} \end{bmatrix} \quad (36)$$

4. SIMULATION RESULTS

The simulation models of non-linear railway wheelset and EKF are developed in Simulink/MATLAB and are simulated 50 microseconds step size. As the vehicle is kept on constant velocity i.e. motor torque is applied zero, only random track disturbance of ±7mm magnitude in lateral direction is applied as input to the model for exciting lateral dynamics. Curves of Figure 2 are tuned with Polach parameters k_A, k_S, u_0, A and B. Table 3 contains the values which are used to tune these creep curves. Along with Kalman gain and Jacobian matrices, the other EKF tuning parameters are measurement noise covariance of inertial sensors and process noise covariance for entire range of track conditions which are set in equation (37)-(40). The measurement noise covariance matrix in equation (37) is calculated by adding noise power for accelerometer and gyro sensor, while the process noise matrices of equations (38)-(40) are calculated based on fine tuning of results.

$$R = [1x10^{-7}\ 1x10^{-13}] \quad (37)$$

$$Q1 = [5x10^{-14}\ 1x10^{-14}\ 1x10^{-14}\ 1x10^{-14}\ 1x10^{-14}] \text{ for dry condition} \quad (38)$$

$$Q2 = [0.5x10^{-12}\ 9x10^{-17}\ 1x10^{-12}\ 1x10^{-12}\ 1x10^{-12}] \text{ for wet condition} \quad (39)$$

$$Q3 = Q4 = [1x10^{-13}\ 9x10^{-17}\ 1x10^{-12}\ 1x10^{-12}\ 1x10^{-12}] \text{ for poor and worst condition} \quad (40)$$

Table 3. Polach parameters.

Parameter	Dry condition	Wet condition	Poor condition	Worst condition
kA	1	1	1	1
kS	1	1	1	1
u0	0.46	0.3	0.2	0.1
A	0.4	0.4	0.1	0.1
B	0.6	0.2	0.2	0.2

http://doi.org/10.17993/3ctecno.2020.specialissue5.279-301

Following tests are performed on wheelset with EKF algorithm.

(i) Dry condition, (ii) Wet condition, (iii) Poor condition, (iv) Worst condition and (v) Transition from dry condition to worst condition.

4.1. DRY CONDITION TEST

The lateral velocity and yaw rate of wheelset as well as creep and creep force are computed along with error on dry condition curve (Dry curve of Figure 2) and shown in Figure 4 to 7.

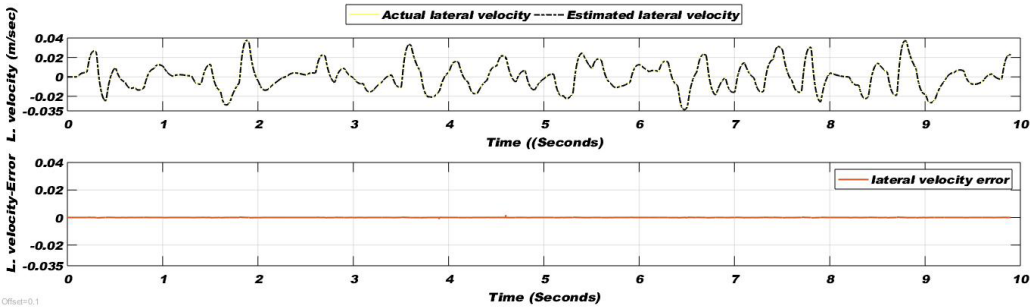

Figure 4. lateral velocity comparison (top) and Error (bottom) for dry condition of wheel-rail interface.

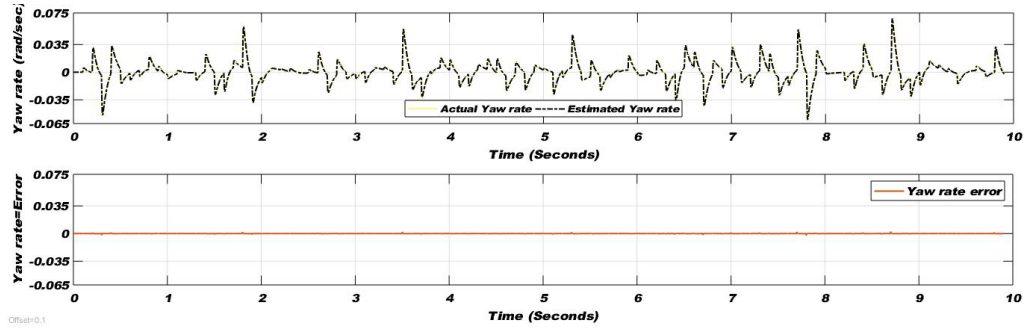

Figure 5. Yaw rate comparison (top) and Error (bottom) for dry condition of wheel-rail interface.

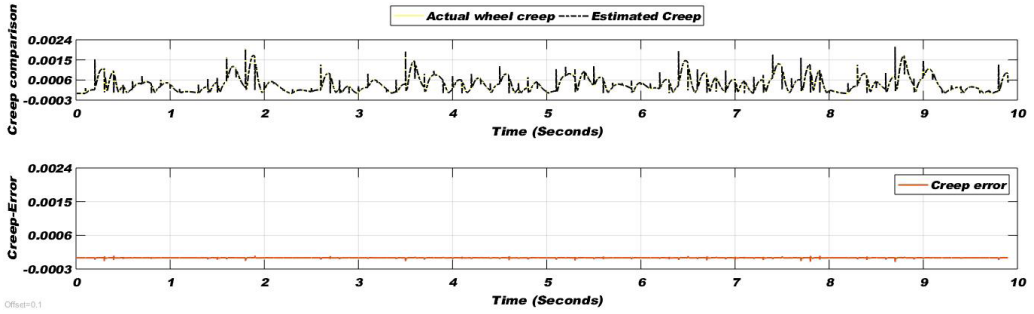

Figure 6. Creep comparison (top) and Error (bottom) for dry condition of wheel-rail interface.

http://doi.org/10.17993/3ctecno.2020.specialissue5.279-301

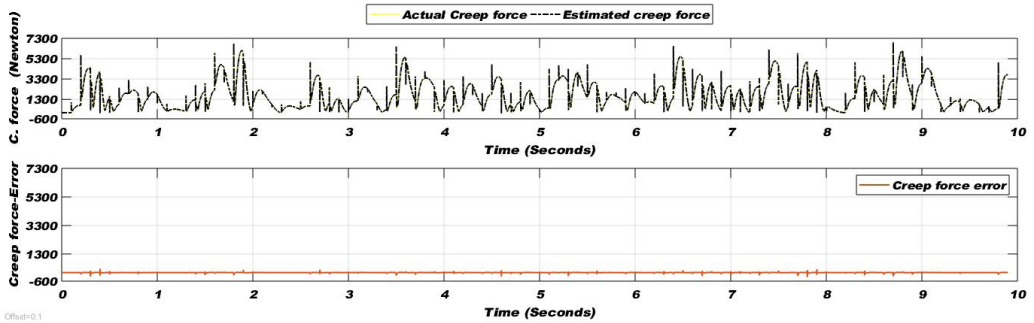

Figure 7. Creep force comparison (top) and Error (bottom) for dry condition of wheel-rail interface.

4.2. WET CONDITION TEST

The lateral velocity and yaw rate of wheelset as well as creep and creep force are computed along with error on wet track condition curve (Wet curve of Figure 2) and shown in Figure 8 to 11.

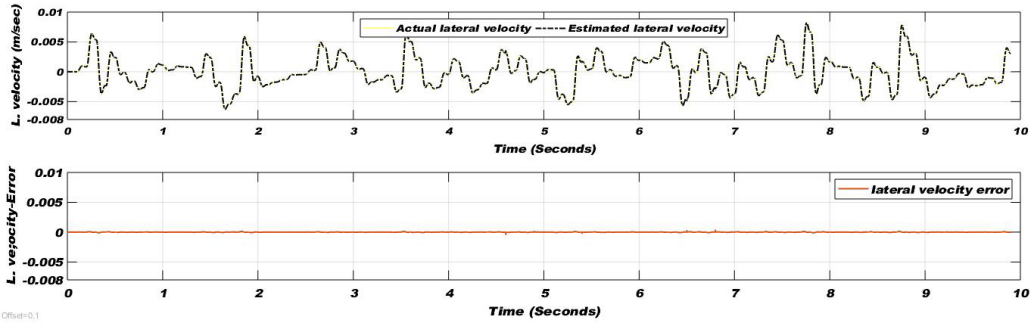

Figure 8. Lateral velocity comparison (top) and Error (bottom) for wet condition of wheel-rail interface.

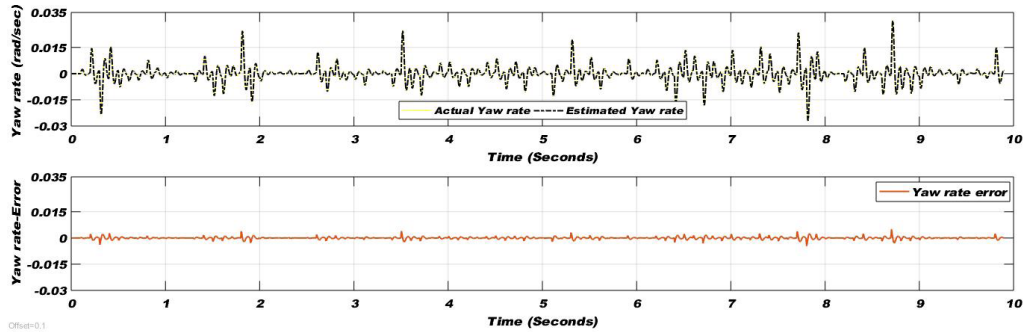

Figure 9. Yaw rate comparison (top) and Error (bottom) for wet condition of wheel-rail interface.

http://doi.org/10.17993/3ctecno.2020.specialissue5.279-301

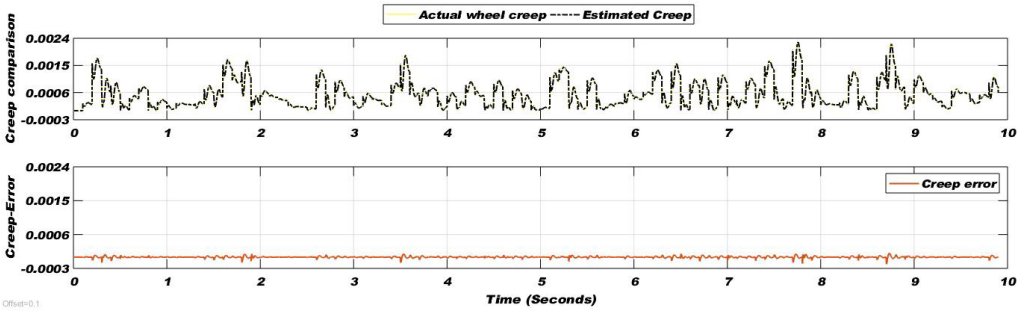

Figure 10. Creep comparison (top) and Error (bottom) for wet condition of wheel-rail interface.

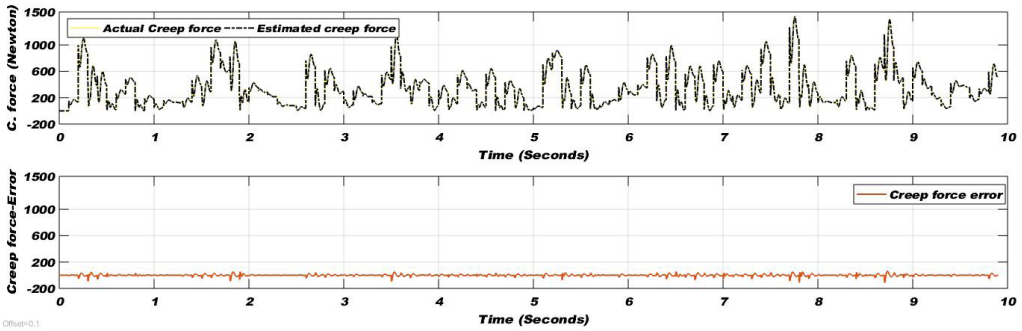

Figure 11. Creep force comparison (top) and Error (bottom) for wet condition of wheel-rail interface.

4.3. POOR CONDITION TEST

The lateral velocity and yaw rate of wheelset as well as creep and creep force are computed along with error on poor track condition curve (Poor curve of Figure 2) and shown in Figure 12 to 15.

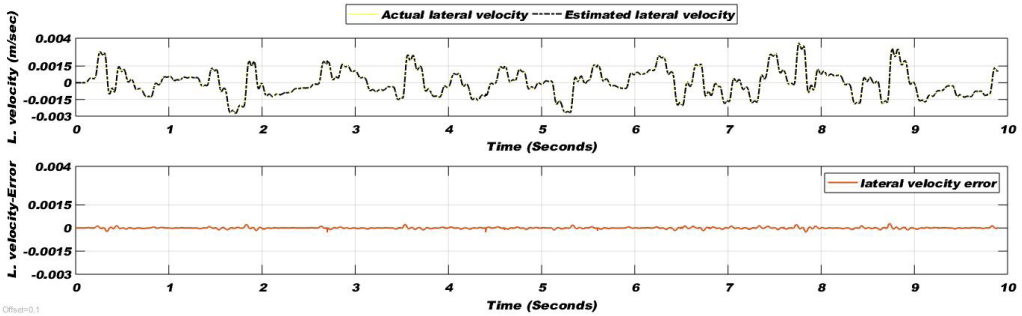

Figure 12. Lateral velocity comparison (top) and Error (bottom) for poor condition of wheel-rail interface.

http://doi.org/10.17993/3ctecno.2020.specialissue5.279-301

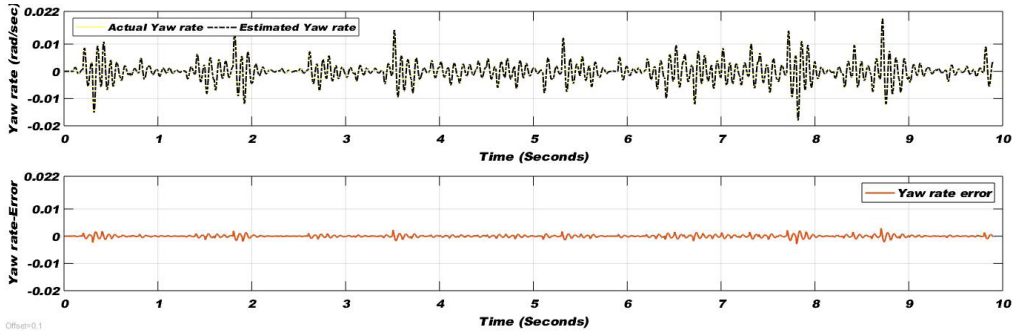

Figure 13. Yaw rate comparison (top) and Error (bottom) for poor condition of wheel-rail interface.

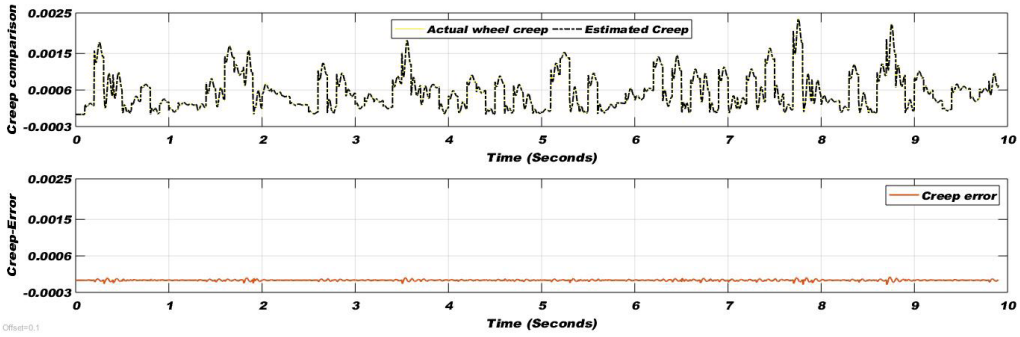

Figure 14. Creep comparison (top) and Error (bottom) for poor condition of wheel-rail interface.

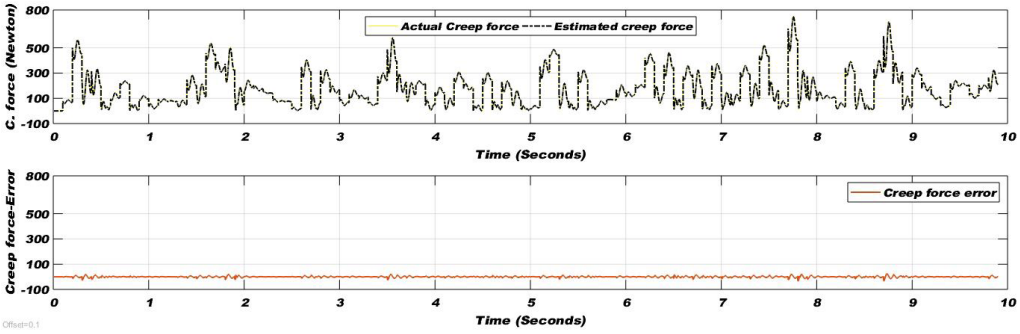

Figure 15. Creep force comparison (top) and Error (bottom) for poor condition of wheel-rail interface.

4.4. WORST CONDITION TEST

The lateral velocity and yaw rate of wheelset as well as creep and creep force are computed along with error on worst track condition curve (Worst curve of Figure 2) and shown in Figure 16 to 19.

http://doi.org/10.17993/3ctecno.2020.specialissue5.279-301

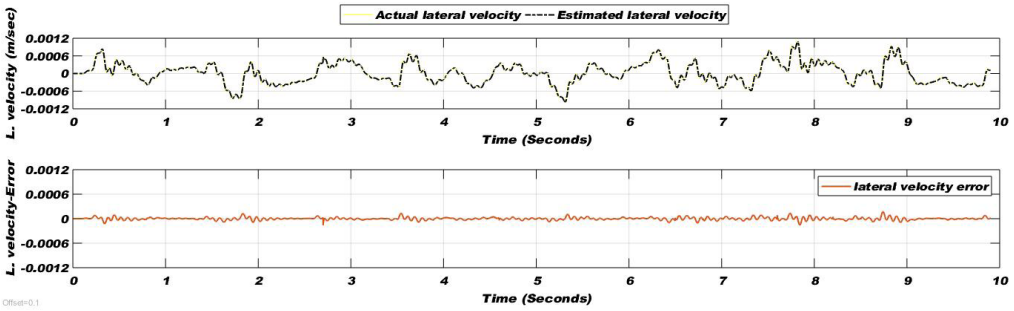

Figure 16. Lateral velocity comparison (top) and Error (bottom) for worst condition of wheel-rail interface.

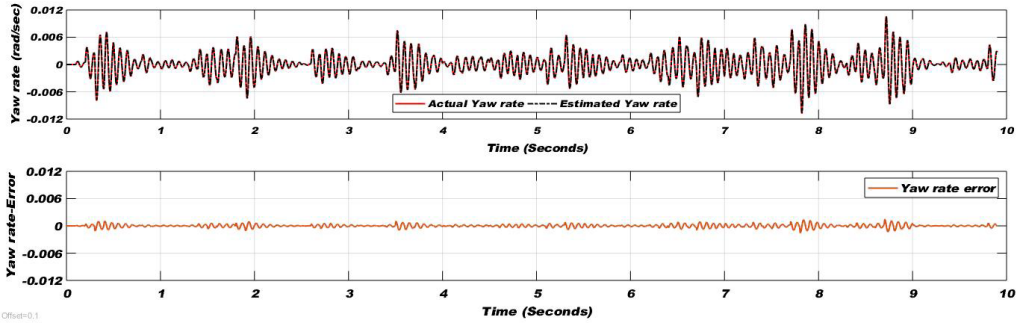

Figure 17. Yaw rate comparison (top) and Error (bottom) for worst condition of wheel-rail interface.

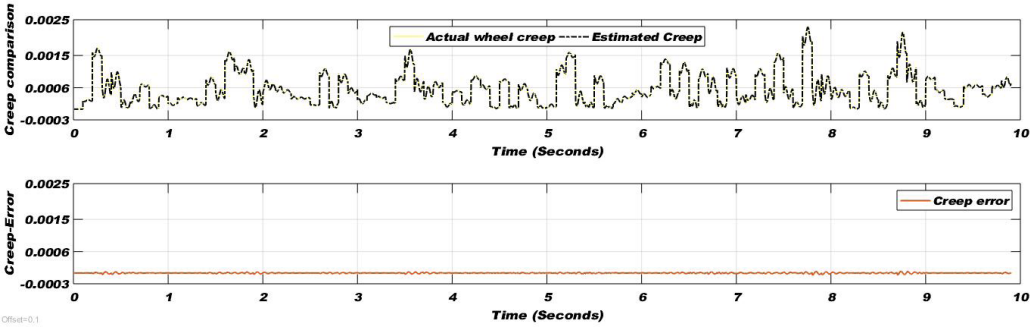

Figure 18. Creep comparison (top) and Error (bottom) for worst condition of wheel-rail interface.

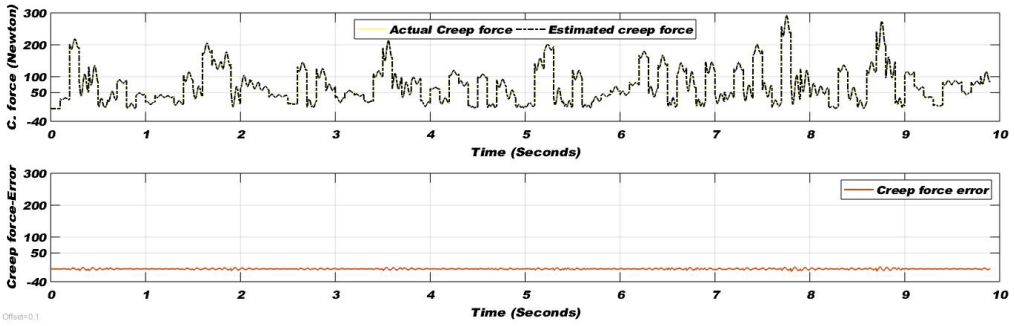

Figure 19. Creep force comparison (top) and Error (bottom) for worst condition of wheel-rail interface.

http://doi.org/10.17993/3ctecno.2020.specialissue5.279-301

4.5. TRANSITION TEST FROM DRY CONDITION TO WORST CONDITION

The lateral velocity and yaw rate of wheelset as well as creep and creep force are computed along with error on all adhesion condition curves (Dry to worst curves of Figure 2) and shown in Figure 20 to 23. During simulation adhesion condition changed at every 2 seconds from dry to worst adhesion conditions in 8 seconds of simulation time and then the condition again changed from worst to wet. The graphs show the changings of adhesion conditions and match estimated results with actual results.

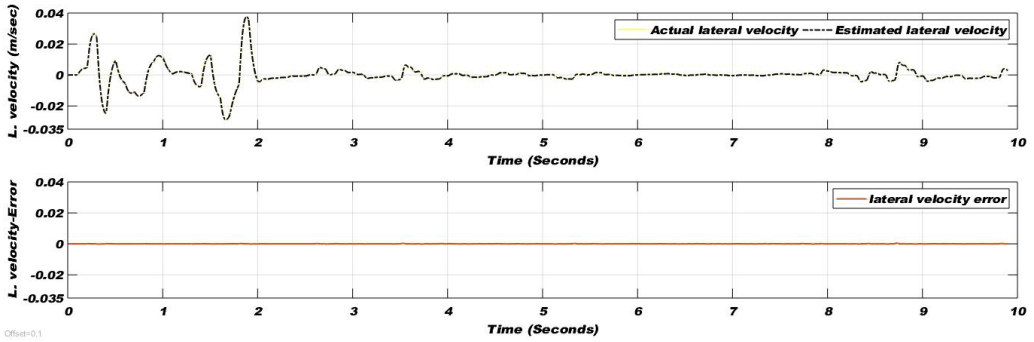

Figure 20. Lateral velocity comparison (top) and Error (bottom) for all track conditions of wheel-rail interface.

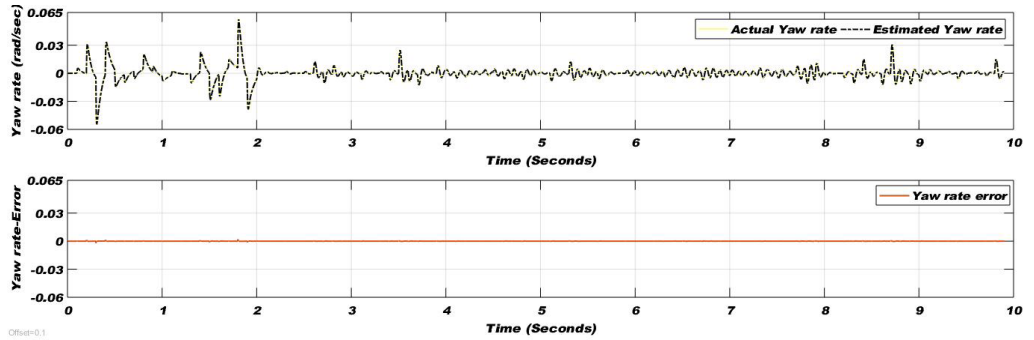

Figure 21. Yaw rate comparison (top) and Error (bottom) for all adhesion condition of wheel-rail interface.

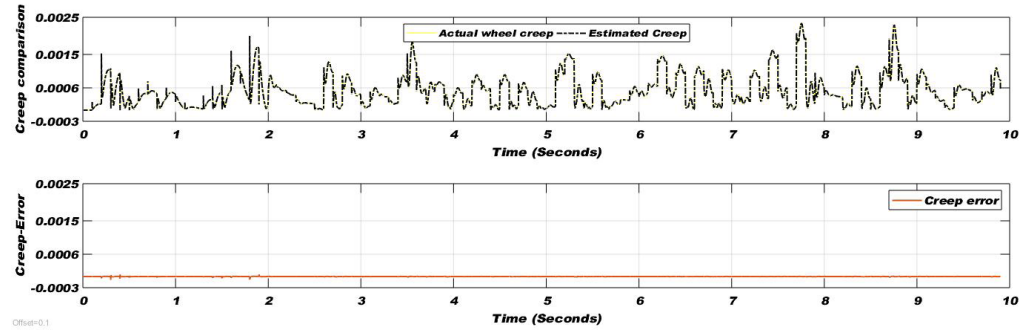

Figure 22. Creep comparison (top) and Error (bottom) for all adhesion condition of wheel-rail interface.

http://doi.org/10.17993/3ctecno.2020.specialissue5.279-301

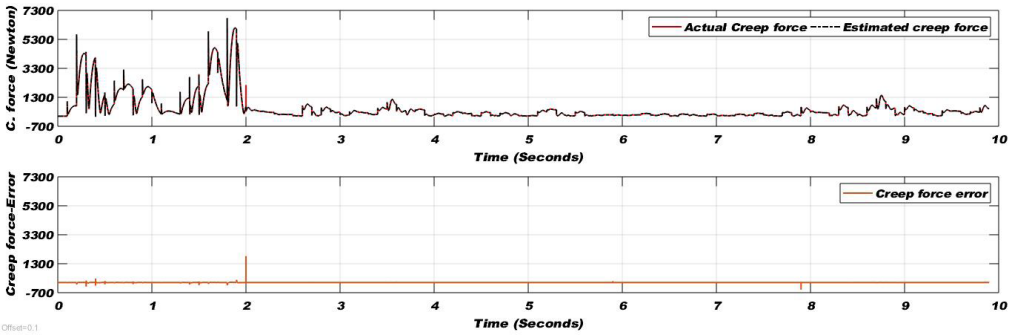

Figure 23. Creep force comparison (top) and Error (bottom) for all adhesion condition of wheel-rail interface.

4.5. ERROR ANALYSIS

It is shown from Figure 4 to 23 that the Extended Kalman filter is a valid estimation technique to estimate wheelset dynamics with authenticity. However, estimated creep force error in Figure 23 became high for few moments during simulation (a spike seen at 2 seconds) due to sudden change of adhesion condition from dry to wet.

Overall, EKF estimates the wheelset dynamics perfectly for dry, wet, poor and worst adhesion conditions and can be used for condition monitoring of rolling stock.

5. CONCLUSION

As wheel-rail contact force is complex and non-linear function of slip and affected with other vehicle parameters, therefore it is difficult to estimate by simple estimating techniques. In this paper, the Extended Kalman filter is used to estimated lateral velocity and yaw rate of railway wheelset as well as creep and creep force of wheel-rail interface and validated through Simulink/MATLAB. EKF estimates not only wheelset dynamics for dry, wet, poor and worst adhesion conditions but perfectly estimates for transition of all track conditions during simulation.

Further, research is going to estimate wheel-rail dynamics in traction and braking modes, also work is going on to implement the simulation work on FPGA platform.

http://doi.org/10.17993/3ctecno.2020.specialissue5.279-301

ACKNOWLEDGEMENT

The authors would like to acknowledge "Condition Monitoring System Lab at Mehran University of Engineering and Technology, Jamshoro, part of NCRA project of Higher Education Commission Pakistan, for supporting their work.

REFERENCES

Anyakwo, A., Pislaru, C., & Ball, A. (2012). A new method for modelling and simulation of the dynamic behaviour of the wheel-rail contact. *International Journal of Automation and Computing*, *9*(3), 237–247. https://doi.org/10.1007/s11633-012-0640-6

Charles, G., Goodall, R., & Dixon, R. (2008). Model-based condition monitoring at the wheel-rail interface. *Vehicle System Dynamics*, *46*(SUPPL.1), 415–430. https://doi.org/10.1080/00423110801979259.

Hubbard, P. D., Ward, C., Dixon, R., & Goodall, R. (2013a). Real time detection of low adhesion in the wheel/rail contact. *Proceedings of the Institution of Mechanical Engineers, Part F: Journal of Rail and Rapid Transit*, *227*(6), 623–634. https://doi.org/10.1177/0954409713503634

Hubbard, P. D., Ward, C., Dixon, R., & Goodall, R. (2013b). Verification of model-based adhesion estimation in the wheel-rail interface. *Chemical Engineering Transactions*, *33*, 757–762. https://doi.org/10.3303/CET1333127

Hussain, I. (2012). *Multiple Model Based Real Time Estimation of Wheel-Rail Contact Conditions* (PhD thesis). University of Salford. http://usir.salford.ac.uk/id/eprint/38094/

Hussain, I., & Mei, T. X. (2010). Multi Kalman filtering approach for estimation of wheel-rail contact conditions. *In UKACC International Conference on CONTROL 2010*. https://doi.org/10.1049/ic.2010.0326

Hussain, I., & Mei, T. X. (2011). Identification of the wheel-rail contact condition for traction and braking control. *Proceedings of the 22nd International Symposium on Dynamics of Vehicles on Roads and Tracks*, *Manchester, United Kingdom*, pp. 14–19. https://www.researchgate.net/publication/261672525_Identification_of_the_Wheel-Rail_Contact_Conditions_for_Traction_and_Braking_control

Hussain, I., Mei, T. X., & Jones, A. H. (2009). Modeling and estimation of non-linear wheel-rail contact mechanics. In *20th International Conference on Systems Engineering (ICSE2009)*, 219–223. https://www.researchgate.net/publication/261633475_Modeling_and_Estimation_of_Non-linear_Wheel-Rail_Contact_Mechanics

Hussain, I., Mei, T. X., & Ritchings, R. T. (2013). Estimation of wheel-rail contact conditions and adhesion using the multiple model approach. *Vehicle System Dynamics*, *51*(1), 32–53. https://doi.org/10.1080/00423114.2012.708759

Mei, T., Yu, J., & Wilson, D. (2008). A mechatronic approach for anti-slip control in railway traction. *IFAC Proceedings Volumes*, *41*(2), 8275-8280. https://doi.org/10.3182/20080706-5-KR-1001.01399

Melnik, R., & Koziak, S. (2017). Rail vehicle suspension condition monitoring - approach and implementation. *Journal of Vibroengineering*, *19*(1), 487–501. https://doi.org/10.21595/jve.2016.17072

Ngigi, R. W., Pislaru, C., Ball, A., & Gu, F. (2012). Modern techniques for condition monitoring of railway vehicle dynamics. *Journal of Physics: Conference Series*, *364*(1). https://iopscience.iop.org/article/10.1088/1742-6596/364/1/012016/meta

Polach, O. (2005). Creep forces in simulations of traction vehicles running on adhesion limit. *Wear, 258*(7-8), 992–1000. https://doi.org/10.1016/j.wear.2004.03.046

Radionov, I. A., & Mushenko, A. S. (2015). The method of estimation of adhesion at "wheel-railway" contact point. In *2015 International Siberian Conference on Control and Communications (SIBCON)*, pp. 1–5. https://doi.org/10.1109/SIBCON.2015.7147156

Simon, I. (2006). *Handbook of Railway Vehicle Dynamics*, *Handbook of Railway Vehicle Dynamics*. CRC Press.

Strano, S., & Terzo, M. (2018). On the real-time estimation of the wheel-rail contact force by means of a new nonlinear estimator design model. *Mechanical Systems and Signal Processing*, 105, pp. 391–403. https://doi.org/10.1016/j.ymssp.2017.12.024

Sun, Y. Q., Cole, C., & Spiryagin, M. (2015). Monitoring vertical wheel-rail contact forces based on freight wagon inverse modelling. *Advances in Mechanical Engineering*, *7*(5), 1–11. https://www.researchgate.net/publication/277910673_Monitoring_vertical_wheel-rail_contact_forces_based_on_freight_wagon_inverse_modelling

Wang, S., Xiao, J., Huang, J., & Sheng, H. (2016). Locomotive wheel slip detection based on multi-rate state identification of motor load torque. *Journal of the Franklin Institute*, *353*(2), 521–540. https://doi.org/10.1016/j.jfranklin.2015.11.012

Ward, C. P., Goodall, R. M., & Dixon, R. (2011). Contact force estimation in the railway vehicle wheel-rail interface. *IFAC Proceedings Volumes, 44*(1), 4398–4403. https://doi.org/10.3182/20110828-6-IT-1002.02904

Welch, G., & Bishop, G. (2001). *An Introduction to the Kalman Filter*. University of North Carolina at Chapel Hill Department of Computer Science Chapel Hill, NC 27599-3175. https://www.cs.unc.edu/~welch/media/pdf/kalman_intro.pdf

Zhao, Y., & Liang, B. (2013). Re-adhesion control for a railway single wheelset test rig based on the behaviour of the traction motor. *International Journal of Vehicle Mechanics and Mobility*, *51*(8), 1173–1185. https://doi.org/10.1080/00423114.2013.788194

Zhao, Y., Liang, B., & Iwnicki, S. (2012). Estimation of the friction coefficient between wheel and rail surface using traction motor behaviour. *Journal of Physics: Conference Series*, *364*(1). https://iopscience.iop.org/article/10.1088/1742-6596/364/1/012004

Zhao, Y., Liang, B., & Iwnicki, S. (2014). Friction coefficient estimation using an unscented Kalman filter. *International Journal of Vehicle Mechanics and Mobility, 52*(suppl. 1), 220–234. https://doi.org/10.1080/00423114.2014.891757

http://doi.org/10.17993/3ctecno.2020.specialissue5.279-301